International Journal of Applied Earth Observation and Geoinformation 141 (2025) 104618

Contents lists available at ScienceDirect

International Journal of Applied Earth Observation and Geoinformation

journal homepage: www.elsevier.com/locate/jag

# Shoreline time series analysis through the Isoradiometric method: Bridging landscape evolution and coastal management

F. Caldareri [a], N. Parrino [a,b,*], L. Balsamo [a,d], G. Dardanelli [c], S. Todaro [a], A. Sulli [a,b], A. Maltese [c]

[a] Department of Earth and Marine Sciences, University of Palermo 90123 Palermo, Italy
[b] Istituto Nazionale di Geofisica e Vulcanologia, INGV, Rome, Italy
[c] Department of Engineering, University of Palermo 90128 Palermo, Italy
[d] Constructional and Environmental Engineering, Sapienza University of Rome, Rome, Italy

ARTICLE INFO

*Keywords:*
Landscape evolution
Shoreline dynamics
Isoradiometric method
Time series

ABSTRACT

The increasing availability of remotely sensed data has enhanced our ability to monitor coastal evolution, yet extracting reliable time series for long-term analysis remains a challenge. This study evaluates the effectiveness of the Isoradiometric shoreline extraction Method in producing consistent time series data across different spatial and temporal scales. We applied the method to about 150 multispectral satellite images spanning 40 years, covering two sandy beaches along Sicily's coast in the central Mediterranean Sea. Our validation approach focused on assessing method consistency across datasets with different spatial resolutions and revisit times. By comparing Landsat and PlanetScope data, we demonstrated that while high-resolution products capture greater variability in shoreline position, lower-resolution but longer time-span observations effectively identify underlying evolutionary trends. The analysis revealed that manual digitization captures instantaneous swash positions, while the Isoradiometric Method consistently identifies stable morphological features between the low tide terrace and berm, providing more reliable indicators of actual coastal change. This multi-resolution approach proved effective in distinguishing between method-related outliers and paroxysmal events, with the latter typically detected across multiple datasets at corresponding timeframes. The systematic application of the Isoradiometric Method successfully characterized both natural variability patterns and anthropic impacts, providing quantitative baselines for interpreting Quaternary coastal processes while offering practical insights for shoreline monitoring and coastal management strategies. Moreover, we calculated the shifts' gradient to quantify the rate of change in shoreline position. These results demonstrate: i) the necessity of creating shoreline time series as a tool for geological interpretation through the principle of actualism and as a framework for rationalizing contemporary shoreline monitoring approaches; ii) the Isoradiometric Method enables accurate Earth Observation image processing for this purpose.

## 1. State of the art

Shorelines' shape and position vary across spatial and temporal scales, driven by the interplay between sediment, wind patterns, current waves, tides, and relative sea-level changes (Burningham and Fernandez-Nunez, 2020). The quantitative understanding of these highly dynamic processes is crucial for geological interpretation and coastal management. These processes give rise to recurring cycles of erosion and sedimentation, which shape modern coastal landscapes forming features such as tidal notches, marine terraces, and river systems (Burbank and Anderson, 2013). Understanding these modern analogues is fundamental to interpreting Quaternary deposits, while also informing coastal management strategies for natural and man-made seaside environment protection (Agate et al., 2024; Parrino et al., 2023, 2022; Srivastava et al., 2023; Luijendijk et al., 2018; Short, 1999).

Recently, many different remotely sensed shoreline extraction techniques have been proposed. These tools allow accurate shoreline detection and monitoring and significantly improve coastal management. These methods can be grouped into three categories (Toure et al., 2019): the edge detection approaches (e.g., Ouyang et al., 2010; Toure

* Corresponding author at: Department of Earth and Marine Sciences, University of Palermo, 90123 Palermo, Italy.
*E-mail address:* nicolo.parrino@unipa.it (N. Parrino).

https://doi.org/10.1016/j.jag.2025.104618
Received 21 January 2025; Received in revised form 14 May 2025; Accepted 21 May 2025
Available online 2 June 2025

et al., 2018) which treat the extraction of shoreline as an edge detection problem; the band thresholding methods (e.g., Otsu, 1979; Aedla et al., 2015) in which a thresholding value is selected either by man–machine interaction or by a local adaptive strategy; the classification approaches (Hannv et al., 2013; Sharma et al., 2015; Gao, 1996; McFeeters, 2013; Costantino et al., 2020) which aim to separate the image into land and water components, and then take the boundary line between them as the shoreline.

### 1.1. Satellite-derived shoreline dynamics analyses

Recent advancements in remote sensing techniques pushed the boundaries of accuracy in shoreline extraction methods for sandy beaches (Almeida et al., 2021; Caldareri et al., 2024; Maltese et al., 2024, 2023; Palomar-Vázquez et al., 2023; Vos et al., 2019a). These investigations focused on remotely sensed shoreline horizontal accuracy (Pardo-Pascual et al., 2018; Wicaksono and Wicaksono, 2019) and temporal variability across different scales (Chen et al., 2022; Murray et al., 2023; Vos et al., 2019b). Indeed, unlike field survey methods and traditional coastal monitoring programs, remote sensing approaches allow fast and precise quantification of shoreline dynamics. This capability is essential not only for studying modern coastal processes but also for developing robust frameworks for both geological interpretation and coastal management decisions, including the planning of effective coastal defence interventions. Satellite-derived shoreline dynamics analyses yielded significant findings regarding erosion and accretion patterns along sandy beaches, one of the most heavily urbanized and exploited regions globally. It allowed to detect that 24 % of the sandy beaches experience erosion at rates exceeding 0.5 m per year while 28 % of the beaches exhibit accretion. Approximately 48 % of the sandy beaches remain stable, showing minimal changes over the analysed period (Luijendijk et al., 2018). These data underscore the dynamic nature of coastal environments and emphasize the importance of monitoring and managing these areas to mitigate erosion impacts and maintain a sustainable balance between stability and natural dynamics. Given the crucial significance of predicting future scenarios of coastal Landscape Evolution (LE), particularly in the context of climatically induced extreme events, the use of remotely sensed time series data has emerged as a pivotal tool (Bengoufa et al., 2021; Boussetta et al., 2023; Gens, 2010; Yasir et al., 2020). This approach enables both the interpretation of long-term geological processes and, through a better understanding of the shoreline dynamics, improves the development of effective coastal management strategies.

### 1.2. Aim and structure of this work

In this research article, we present a critical analysis of the outcomes achieved through an application of the Isoradiometric shoreline extraction Method (hereinafter, the IM) proposed by Caldareri et al. (2024) and Maltese et al. (2023), Maltese et al. (2024) across a comprehensive dataset. Our approach focused on analyzing shoreline dynamics through time series, aiming to quantify and interpret coastal LE, which is constantly hampered by natural and anthropic forcings. In this article, we explore the use of the IM as a potential solution to this issue. The goals of this research are:

- to highlight the effectiveness of time series in analyzing coastline evolution;
- to demonstrate that the time series produced by IM are high-quality products suitable for coastal landscape management.

The study was carried out on two sandy beaches located on Sicily Island which exhibit comparable daily tide excursions, ranging from 11 to 30 cm while showcasing distinct hydrodynamics energy variations. Through Earth Observation data systematic processing, we demonstrated how shoreline evolution patterns provide insights into various processes, including sedimentary dynamics, anthropogenic influences, and climatic factors, considering their spatial and temporal wavelengths.

In this paper, we will begin with a description of the areas under study and the datasets of satellite products used. We will proceed with an account of the method used describing advantages and issues. We then present the results obtained from the processing of multispectral images, with a focus on pair analysis to quantify the influence of satellite product resolution on shoreline variability estimation. Then we will illustrate the results of seasonal and multidecadal analysis up to the realization of the time series which will also allow us to highlight the limitations and potentialities of the datasets used. Finally, we will discuss the results emphasizing how this method can be used to understand coastal dynamics through the realization of time series and the recognition of temporal and spatial patterns. Moreover, we speculate on the drivers of coastal LE and the method potentialities for coastal management by tracing the direction of future developments.

## 2. Material and methods

### 2.1. Study region

This study focuses on sandy beaches along the Sicily Island coast of the Central Mediterranean basin (Fig. 1A, B). As case studies, we chose San Giorgio (Fig. 1C), located in the northern sector, of which we analysed about 12 km of sand-gravel beach with an average width of 40 m and facing the Tyrrhenian Sea. On the eastern coast, we selected the Vendicari beach (Fig. 1D), of which we analysed about 6 km of sandy coast with an average width of 35 m, facing the Ionian Sea. These beaches encompass two distinct study sites that exhibit different characteristics ranging from the geological composition of the surrounding area, the orientation of the beaches, the protection level compared to surface currents and prevailing winds, grain size variations (spanning from a D50 of 0.48 mm for the Vendicari beach to a D50 value of 2.8 mm in San Giorgio study case) and the anthropogenic footprint (e.g. harbours and coastal defence structures such as groynes). Despite these variations, the two study sites share a common microtidal regime, characterized by relatively small tidal ranges from 11 to 30 cm. This consistent tidal regime provides a valuable baseline for comparative analysis and allows for a focused investigation into the specific dynamics of every beach.

### 2.2. Dataset

In this analysis we used two distinct satellite datasets, Landsat and Planetscope, to acquire comprehensive information spanning over a period of up to 40 years (Figs. 2 and 3A1-2). The Landsat dataset encompasses the Thematic Mapper (TM), Enhanced Thematic Mapper + (ETM + ), and Landsat Operational Land Imager (OLI) images from the Level 2 Collection 2 Tier 1, for further information see: https://www.usgs.gov/media/files/landsat-collection-1-vs-collection-2-summary). It offered a geometric resolution of 30 m and, due to the exceptional longevity of the program, it was suitable for time-series analysis (USGS, 2017). We processed Landsat 5 TM images from 1985 to 2010, Landsat 7 ETM + images for 2011 and 2012, and Landsat 8 OLI images from 2013 to 2022. Additionally, commercial satellite products from Rapid Eye and Planetscope satellite constellations have been processed, specifically the images acquired by the Rapid Eye JSS56, with a geometric resolution of 5 m and Planetscope Dove R sensors, operated by Planet, with a geometric resolution of 3 m, were processed for the years 2009 to 2022 (Image © 2019–2022 Planet Labs PBC).

Furthermore, aerial orthophotos accessed through the Web Map Service (WMS) provided by the Italian National Geoportal under the Ministry of the Environment and Energy Security (Geoportale Nazionale, Ministero dell'Ambiente e della Sicurezza Energetica, https://gn.mase.gov.it/portale/servizio-di-consultazione-wms) and satellite

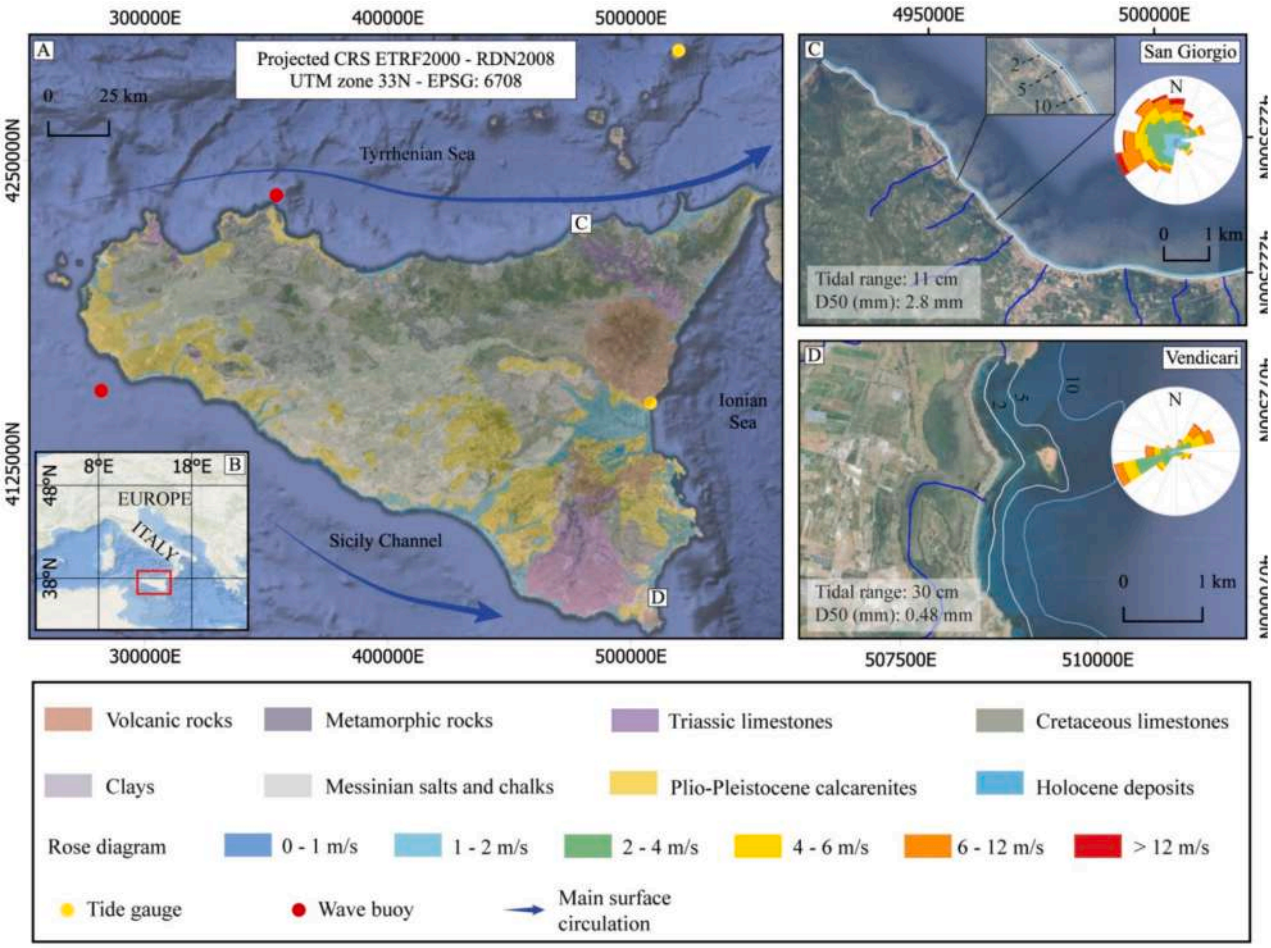


**Fig. 1.** (A–B) Geographical Setting of the two study sites on Sicily Island: the map illustrates the locations, providing a comprehensive overview of their geographical distribution. San Giorgio beach (C) is situated in the north-eastern sector, while Vendicari (D) is positioned along the eastern coast. Inset A provides the locations of the tide gauge and wave buoy, the main surface current circulation is represented with the blue arrow. Insets C and D provide information on tidal range, median sediment grain sizes (D50) and the rose diagram of the prevailing wind direction. (For interpretation of the references to colour in this figure legend, the reader is referred to the web version of this article.)

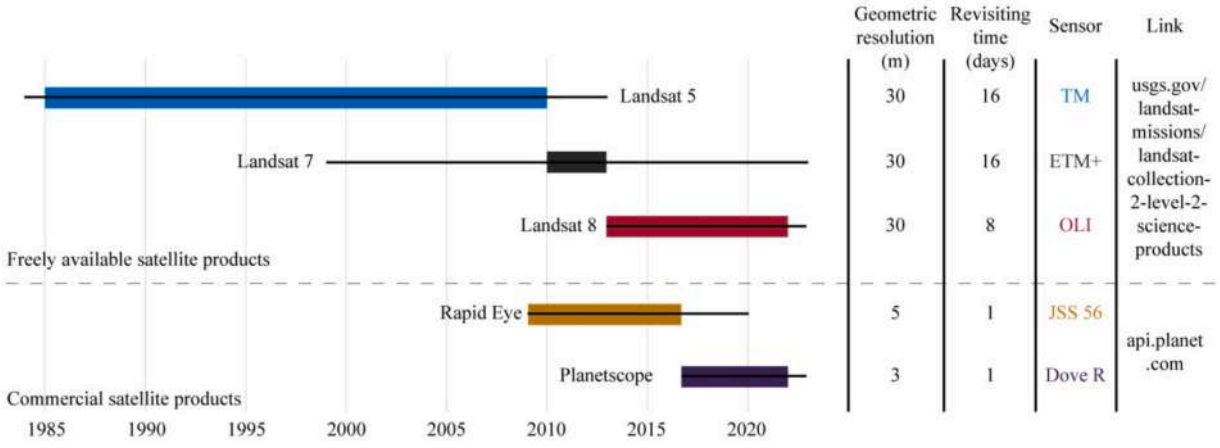


**Fig. 2.** Timeline of the processed satellite products. The black lines represent the operating period of the satellite missions, while the coloured boxes indicate the sensing period of the satellite products employed in our research. The geometric resolution, revisiting time, and sensor information for both public and commercial satellite missions are provided in the right columns for reference.

orthophotos obtained via the Google Earth Professional platform were employed to evaluate the accuracy of the time series. Multidecadal time series were validated by processing nine images acquired on 07/1997 (the metadata does not include information regarding the date of acquisition), 13/05/1999, 28/08/2005, 08/08/2010, 09/07/2012, 06/06/2014, 14/06/2017, 10/06/2018, and 24/05/2020, while the seasonal time series were validated by processing two images acquired on 11/05/2022 and 24/04/2023.

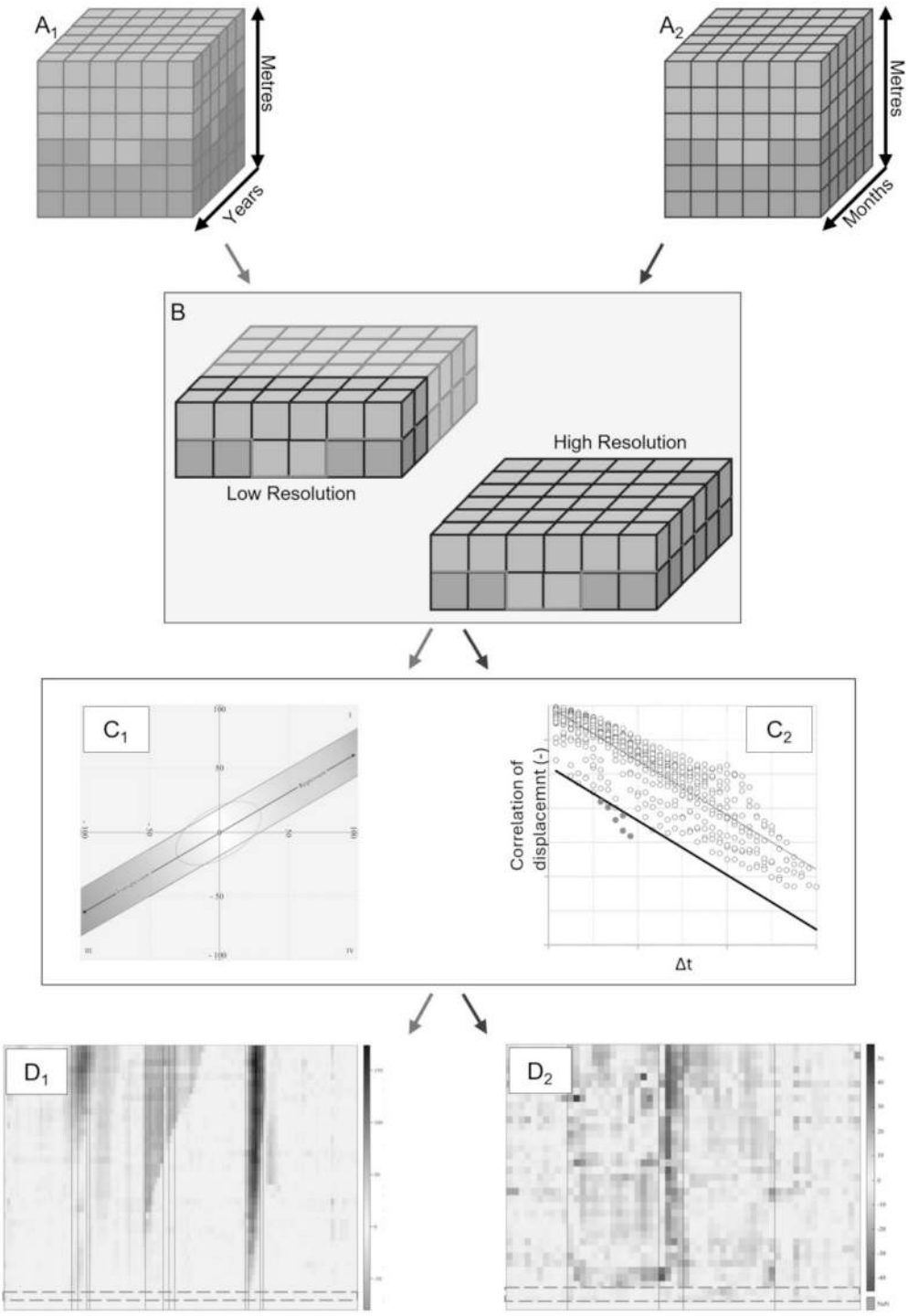


**Fig. 3.** $A_1$) Data-cube of low-resolution satellite products starting from 1985 to 2022, and $A_2$) of high-resolution satellite products starting from 2009 to 2022. The x-axis shows the time-span, and the y-axis shows the horizontal displacement; B) Extracted shorelines by mean of ISE application; C1) Pairwise analysis used to identify method criticalities (outside the confidence band); C2) Pairwise analysis to identify outliers correlation'; D1) San Giorgio beach multidecadal time series heatmap; D2) Vendicari beach seasonal time series heatmap. The arrows indicate the consequentiality of the analyses carried out.

### *2.3. Methods*

We present a systematic application of the Isoradiometric Method (IM) proposed by Caldareri et al. (2024, Fig. 3), a novel sub-pixel resolution approach that treats pixels as concurrent radiometric acquisitions on a square grid. This method extracts shorelines from remotely sensed images of sandy beaches by leveraging the radiometric signature difference between water and sand and identifying an isoradiometric line to represent the physical shoreline. The IM identifies shoreline position by calculating the minimum distance between two consecutive isolines of reflectance.

Caldareri et al. (2024) demonstrated that the IM has passed multiple validation tests examining accuracy for specific spectral bands and spatial resolutions, spectral signature behaviour, water depth attenuation effects, georeferencing accuracy, and grain size sensitivity. When compared with other methodologies in the literature, IM demonstrates

superior accuracy and avoids the classic sawtooth morphology typically associated with pixel-based methods due to its subpixel resolution capabilities. Preliminary testing has been conducted on various imagery types, including spectral reflectance in the sunlight range, surface temperature in the thermal infrared, and backscattering in the microwave (Maltese et al., 2023; Maltese et al., 2024).

The primary focus of our research is generating time series datasets that enable spatial and temporal interpretation of morphodynamic drivers influencing shoreline changes. By applying the IM to two different resolution satellite product dasatests (Fig. 3A1-2), allowed us to perform an accuracy comparison (Fig. 3B) and the pairwise analyses which led us to distinguish between shift outliers resulting from IM methodological limitations and changes associated with genuine paroxysmal events (Fig. 3C1-2). The resulting datasets illustrate potential driving factors of coastal change, whether natural or anthropogenic in origin (Fig. 3D1-2).

Our methodological workflow produced a series of polylines representing shoreline positions at the time of satellite image acquisition (Fig. 4A). To facilitate systematic analysis and meaningful comparisons, we established a landmark shoreline for each study site based on the shoreline position as of July 2022. Using this reference, we constructed perpendicular transects intersecting the landmark shoreline at regular intervals of approximately 100 m, extending 200 m perpendicular to the landmark. Each transect was uniquely identified with an increasing numerical label.

We calculated along-transect measurements using the intersection points between these transects and the extracted shorelines, determining distances between each point and the established landmark shoreline. As illustrated in Fig. 4B, we adopted the convention where negative values indicate sea transgression (landward shoreline movement) and positive values represent sea regression (seaward movement). This standardized approach ensured consistency and facilitated the interpretation of shoreline dynamics relative to the reference shoreline.

To identify and emphasize the most significant shift values and effectively represent natural variability in the data, we classified the transects using the Jenks natural variance classification algorithm (Jenks and Caspall, 1971). This approach minimizes variance within each group while maximizing variance between groups, creating distinct classes with enhanced internal similarity.

### 2.3.1. *Pairwise analysis and statistical approach*

To ensure robust comparisons, a pairwise analysis was performed using images acquired (as possible) simultaneously but at varying spatial resolutions, to identify and handle outliers in our dataset. Outliers caused by method criticalities generally occur outside the confidence band; however, criticalities that remain stable over time and appear consistently across different resolutions may be found within the confidence band but outside the confidence ellipse. Similarly, outliers resulting from genuine extreme events typically appear outside the confidence ellipse within the confidence band. We analyzed the statistical distribution of shifts and isolated potential outliers for separate examination (Figs. 5 and 3C1). In the current implementation of our algorithm, method criticalities are identified automatically using confidence bands, while shifts identified by confidence ellipses require case-by-case analysis.

Given that shoreline changes occur at different temporal scales, we implemented two complementary analytical approaches to capture significant variations beyond daily or monthly fluctuations. Tidal variations, while present, were considered not significant for our purposes and incompatible with the revisit time of the satellite platforms used in

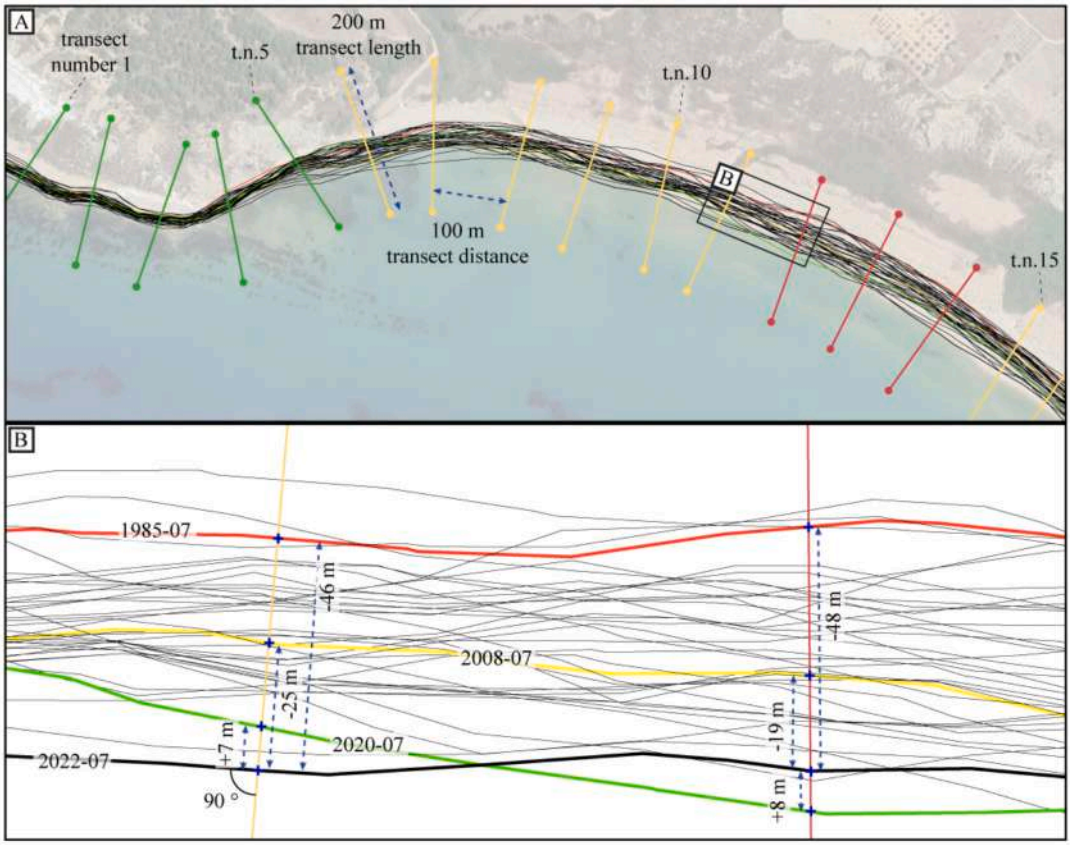


**Fig. 4.** A) San Giorgio Beach section: shorelines extracted from the Landsat satellite product are depicted as black lines, while coloured lines denote perpendicular transects positioned along the shoreline. Transects colours correspond to the Jenks natural breaks classification. B) A closer view of what shown in inset A), focusing on a landmark shoreline (black line). This shoreline serves as a reference for calculating shifts observed in all other shorelines.

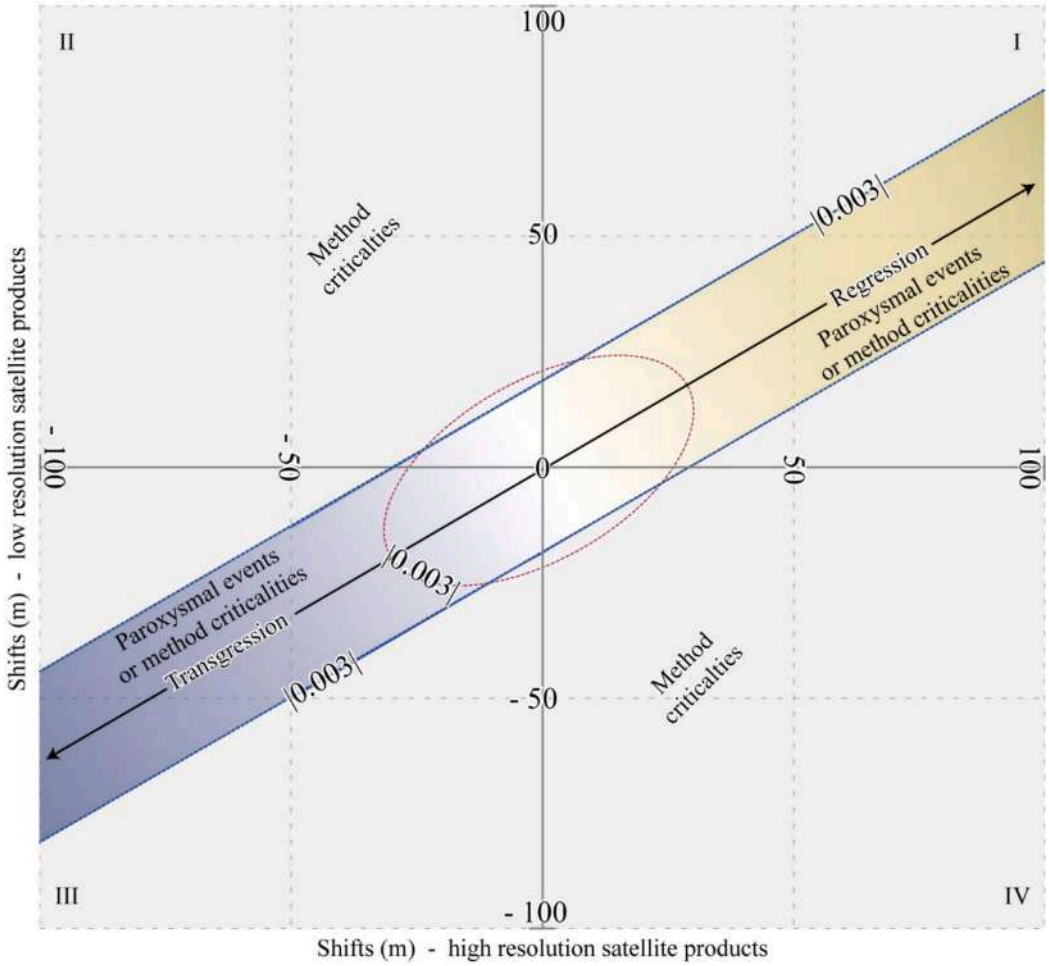


**Fig. 5.** In the x-axis, the shifts (in m) of the lowest geometric resolution satellite products are shown while the shifts of the highest geometric resolution satellite products are shown in the y-axis. The confidence band with graduated colours with a value of 0.003, shows positive values in the first quadrant (sea regression) and negative values in the third quadrant (sea transgression). Values found at the extremes of the band are those linked to paroxysmal events. The pairs outside the band, in the grey area, are interpreted as method criticalities (outliers). The dotted red line represents a confidence level of 0.003. (For interpretation of the references to colour in this figure legend, the reader is referred to the web version of this article.)

this study (Masselink and Short, 1993). Our dual approach consisted of:

Seasonal Analysis: Using PlanetScope (PS) satellite products, we selected one image per month over three years to capture short-term fluctuations.
Multi-decadal Analysis: Using Landsat (LS) satellite products, we selected one image per year spanning approximately 40 years to observe long-term trends.

To characterize the statistical nature of shoreline shifts across different resolutions, we fitted probability density functions to the measured shifts. The Anderson-Darling statistic (AD; D'Agostino and Stephens, 1986) was employed to assess how closely the data followed specific distributions, with smaller AD values indicating better fits. This analysis provided insights into how different resolution datasets capture paroxysmal events.

In the analysis of displacement shifts, probability density functions were employed to model the data derived from the datasets at different spatial resolutions. The Normal and Smallest Extreme Value (SEV) (Kotz and Nadarajah, 2015) distributions were identified to characterize shifts at coarse and fine resolutions (e.g. Benetazzo et al. (2020)) use extreme value distributions to model extreme marine events, specifically focusing on maximum wave heights and maximum crest heights during marine storms.

### 2.3.2. Validation methodology

While the accuracy of IM-extracted shorelines was previously validated by Caldareri et al. (2024) using GNSS techniques, we implemented additional validation protocols for our time series analysis. Since our analysis covered historical periods, we compared IM-extracted shorelines with manually digitized shorelines from high-resolution archival satellite images available on the Google Earth Professional platform even if the temporal mismatches between validation imagery and satellite acquisitions are unaddressed, risking reducing the accuracy claims in micro-tidal settings. The digitization process followed the methodology described by Pipitone et al. (2018). For the Protocols detailed description refers to Supplementary Materials (S.1 and S.2).

Our validation focused on measuring distances between vertices of digitized shorelines and those extracted by the IM. To ensure temporal consistency, we only considered images acquired within approximately two months of the corresponding satellite acquisition for validating multi-decadal time series, and within the same month for seasonal time series. This approach allowed us to assess the reliability of our shoreline extraction method across different temporal scales while accounting for historical data limitations.

To evaluate the planimetric accuracy of orthophotos, statistical values were extracted and analyzed. Interquartile range (IQR) and standard deviation (σ) were calculated for distance matrices, distinguishing between aerial orthophotos accessed via the Web Map

Service (WMS) and satellite images accessed through the Google Earth platform.

## 3. Results

By systematic application of the IM proposed by Caldareri et al. (2024), we processed a total of 148 multispectral satellite images, covering approximately 18 km of sandy beaches. This time series approach allowed us to extract a dataset consisting of a shoreline for each image and obtain a total of 13,024 shift measurements collected along 176 transects within the identified study areas over the past 40 years. Out of the 13,024 measurements, a total of 1124 amounts were due to critical issues associated with the IM. These issues included double measurements or other criticalities. As a result, we were able to perform pair analysis on 11,900 pairs of shift measurements. In these pairs, we identified 219 outliers (interpreted as method criticalities), 137 measurements related to paroxysmal events, and 11,544 measurements associated with the normal variability of the shoreline for each analysed site. By analysing the shift measurements transect by transect, we categorized the shift values into three distinct Jenks classes of variance. This classification resulted in 1201 values assigned to the maximum variance class, 4282 values to the intermediate variance class, and 7653 values to the minimum variance class. We calculated the shifts' gradient to quantify the rate of change in shoreline position revealing a maximum averaged positive gradient of 13.15 m/yr, indicating the highest rate of seaward movement or accretion observed. The mean value of the positive gradient was 1.22 m/yr. Additionally, we identified a maximum negative gradient of −5.38 m/yr, representing the highest rate of landward movement or erosion recorded. The mean value of the negative gradient was −0.63 m/yr. These gradient values provide valuable insights into the magnitude of shoreline changes within the study areas.

### 3.1. Pairwise analysis

Three confidence ellipses were calculated at different confidence levels (0.3173, 0.0455 and 0.003 for the inner thick red line to the outer thin red line, respectively). Analysing the dispersion of the shifts at different spatial resolutions (Figs. 6 and 3C2) enables us to quantify the influence of the resolution on the estimate of shoreline variability. The shifts obtained at the lowest spatial resolution (y-axis) in all three cases show a range of variability lower than the ones obtained at the highest resolution (x-axis).

Green points represent shifts calculated from datasets at different resolutions that show proportionality shifts that could be considered congruent at different resolutions. Instead, the red points are assumed as possible outliers and were identified in the portions of the beach in which criticalities of the method emerge, for instance, due to shadows.

The two probability density functions that best fit the shifts determined using the Landsat and Planetscope datasets are the Normal and the Smallest Extreme Value (SEV) distributions (Fig. 7, Kotz and Nadarajah, 2015). The normal distribution best fits the shifts distribution at the coarsest resolution (Landsat, AD = 248 for the normal distribution, vs. AD = 550 for the SEV distribution), while the SEV distribution better fits the shift at the finest resolution (Planetscope, AD = 550 for the normal distribution vs. AD = 348 for the SEV distribution). The adaptation to the law of frequency distribution shows that the displacements derived from the Landsat images are well described by the Gaussian distribution, while those derived from the Planetscope images are better described by the SEV distribution. This corroborates the inference that high-resolution images may be more suitable for accurately capturing displacements due to paroxysmal events. For a detailed description refers to Supplementary Materials (S.3).

### 3.2. Pairwise Pearson correlation on seasonal and multidecadal analyses

Fig. 6 shows the correlations, $r$ (−), between the shifts of two pairs of years spaced by a time-lag Δt (yellow points). The correlations tend to decrease as the time lag in years increases (dashed trend line). Fixed the Δt against which we evaluate the correlation, we see that most of the pairs have high values, however, low values are also noted. The pairs outside the confidence band have been represented with their correlation in Fig. 8.

The pairs in red and outside the confidence band refer to the pairs of years 2020–2010, 2021–2010, 2021–2011, 2021–2012, 2021–2013, and 2021–2014, with correlations of (0.357, 0.237, 0.269, 0.331 0.405, 0.438), respectively, with the year 2021 recurring. Fig. 6C shows the correlations, $r$ (−), between the shifts of two pairs of months spaced by a time-lag $\Delta t$ (red points). The correlations tend to decrease as the time lag (expressed in months) increases, as seen in the Vendicari case study analysed using PS (dashed trend line). Once an interval has been chosen for characterizing the evolution of the shoreline—10 years being a typical value—the selection of one pair over another results in shorelines that exhibit significantly different correlations. This underscores that time series with high temporal frequency provide more comprehensive information compared to monitoring conducted at less frequent intervals, which offer only partial information. The pairs in red and outside the confidence band refer to the months 06/2022—11/2021,

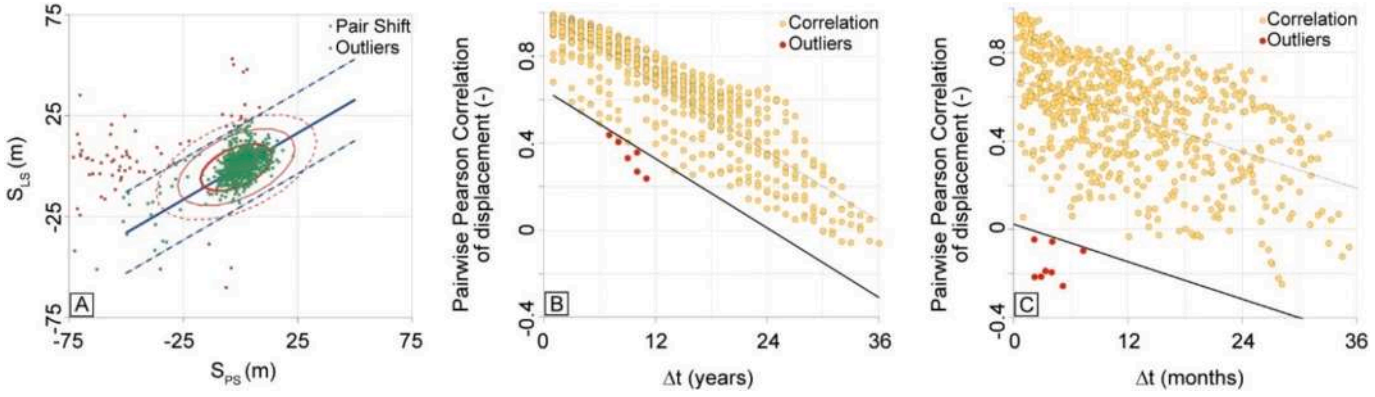


**Fig. 6.** A) Comparison of the shoreline shifts (S) estimated by satellite products. The x-axis represents the shift values at the finest resolution (Planetscope), while the y-axis represents the shift values estimated at the coarsest resolution (Landsat). The trend line is shown in black. Refer to the Fig. 5 for graph details. B) Pairwise Pearson Correlation as a function of the yearly time-lag (yellow point) on the San Giorgio beach. Highlighted in red are the pairs showing a correlation smaller than the lower boundary (a = 0.003). C) Pairwise Pearson Correlation as a function of the monthly time lag (yellow point) on the Vendicari beach. Highlighted in red are the pairs showing a correlation smaller than the lower boundary (a = 0.003). (For interpretation of the references to colour in this figure legend, the reader is referred to the web version of this article.)

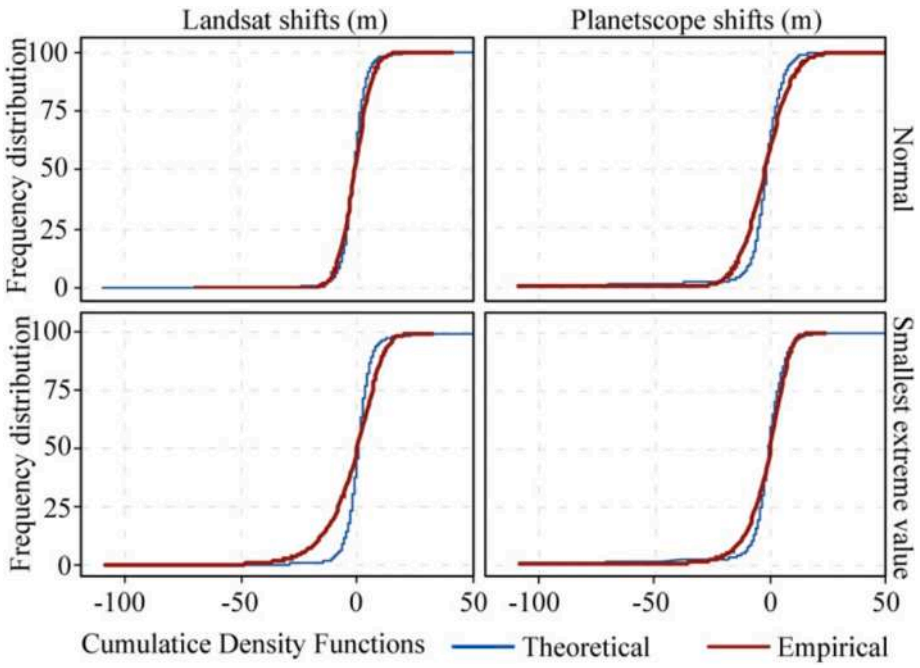


**Fig. 7.** Normal and smallest extreme value cumulative density functions (CDF) are shown in the upper and lower panels, respectively. The shifts determined from Landsat and Planetscope data are displayed in the left and right columns, respectively. Theoretical CDFs are represented by blue lines, while empirical CDFs are represented by red lines. (For interpretation of the references to colour in this figure legend, the reader is referred to the web version of this article.)

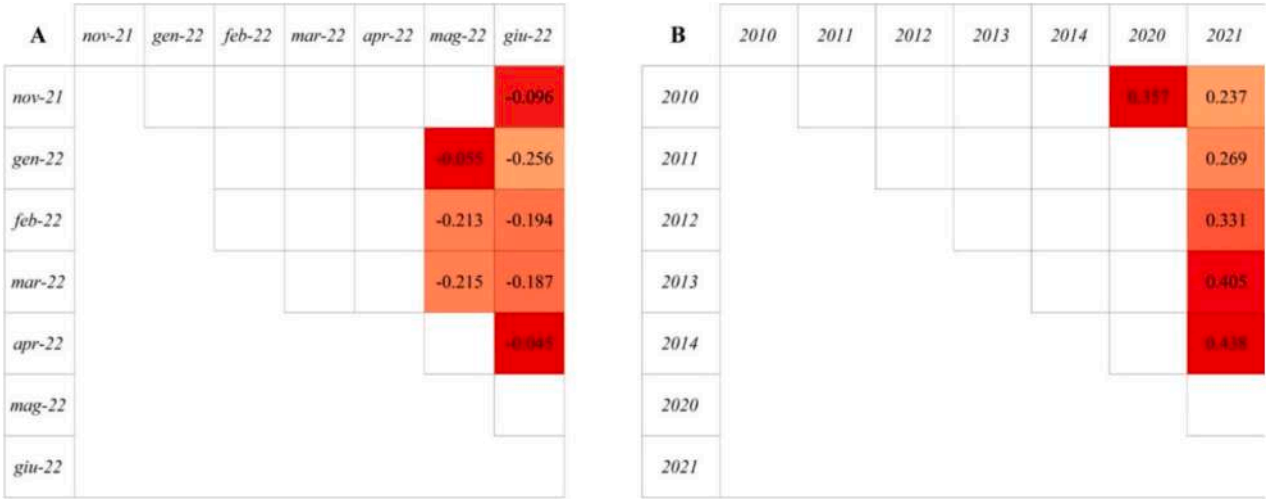


**Fig. 8.** Outliers of the correlation analysis: (a) Seasonal analysis; (b) Multidecadal analysis.

05/2022—01/2022, 06/2022—01/2022, 05/2022—02/2022, 06/2022—02/2022, 05/2022—03/2022, 06/2022—03/2022, 06/2022—04/2022 with correlations of −0.096, −0.055, −0.256, −0.213, −0.194, −0.215, −0.187, and −0.045 with May and June 2022 recurring months, respectively.

### 3.3. Time series case histories

In our comprehensive exploration of the dataset, obtained through the application of the IM, our focus was on the examination of the evolution of the shoreline in the investigated case histories. The following paragraphs present the time series outcomes, focusing on the limitations and potential of the dataset. These outcomes consider various parameters, including the Sicilian coastal sector, satellite products, time series type, beach morphodynamics drivers, and the specific sandy beaches investigated (see Table 1). First, we present the outcomes of a seasonal analysis (on the Vendicari beach), then the outcomes of a multidecadal analysis (on the San Giorgio beach). The latter beach faces the Tyrrhenian Sea (North) while the Vendicari beach faces the Ionian Sea (East). For the seasonal analyses, we employed the Planetscope archive, while for the multidecadal analysis was used the Landsat archive.

**Table 1**
Time series case characteristics for the beaches of Vendicari (VD) and San Giorgio (SG).

| Parameters / Localities | VD | SG |
|---|---|---|
| Sicilian Coastal Sector | E | N |
| Satellite datasets | Planetscope | Landsat |
| Time Series | Seasonal | Multidecadal |
| Beach morphodynamics driver | Sediment flux | Anthropic |

Hereafter, the percentage of measurements acquired from different satellite platforms in both the multidecadal, and seasonal analysis are shown (Table 2), to assess the contribution of each platform to the total dataset and evaluate the reliability and coverage provided by different satellite platforms in capturing shoreline dynamics over time. The above-mentioned archives allow covering a percentage of the designed time series depending on the satellite revisit time.

Landsat emerged as the most reliable archive for the multidecadal analysis (86 %), while Planetscope demonstrated superior performance for the seasonal analysis (97 %). Vendicari Beach was examined using a seasonal time series of Planetscope images over a three-year period with monthly frequency. Regarding the validation of the time series, Table 3 presents statistical indices characterizing the distances between digitized vertices and shorelines extracted using the IM. Approximately 500 vertices were validated, with a majority distance (*Mo*) of 0.30 m on average (ranging from 0.14 to 0.45 m), while the average distance ($\mu$) indicates a lower performance of the IM, with a range of variability from 3.7 to 5.2 m. The interquartile range (IQR) was 3.7 m on average, and the standard deviation of the distances ($\sigma$) was 3.2 m on average. The dataset used for this validation is freely available in the repository at the following link: https://zenodo.org/records/14711106.

Vendicari Beach is characterized by significant shoreline variability as indicated by the measured shifts. The maximum variance of $\approx$ 56 m and the minimum variance of $\approx -45$ m highlights the range of changes observed along the shoreline. These variations have been categorized into three distinct classes: Jenks Class 1, Jenks Class 2, and Jenks Class 3, hereafter J1, J2 and J3 (Figs. 9 and 3D2).

J1 shows the highest and lowest values of $\approx$ 23 m and $\approx$ 20 m, respectively, indicating moderate changes while, J2 exhibits a wider range, with a maximum of $\approx$ 56 m and a minimum of $\approx -44$ m, suggesting more substantial shifts in the shoreline. Class J3 demonstrates a maximum value of $\approx$ 40 m and a minimum value of $\approx -45$, representing the most extreme changes observed in the study.

The monthly displacement gradient along the transects (Fig. 10) exhibits regression fluctuations interspersed with periods of transgression, predominantly occurring on a bimonthly and quarterly basis. Quite distinct behaviours are observed in the two bays located to the north and south of the sandbar. The San Giorgio Beach was studied through a multidecadal time series of Landsat images over nearly four decades with yearly frequency. Regarding the validation of the time series, Tables 4 and 5 present statistical indices characterizing the distances between digitized vertices and shorelines extracted using the IM.

Three campaign-level structures were selected for the placement of GCPs. The GCPs exhibit the following average geographic coordinates in EPSG 6706: (38.1537, 14.9646), (38.1709, 14.9444), and (36.7704, 15.0858). Approximately 240 reciprocal distances were calculated. Average statistical values between the three GCPs were evaluated for all images, distinguishing between the aerial orthophoto accesses via WMS and the satellite images accessed via the Google Earth platform.

The statistical values extracted from aerial orthophotos (see Table 4 reporting "Orthophoto planimetric accuracy") demonstrate reduced accuracy, and behaviour consistent with the average statistical indicators of their accuracy (see following Table 5 reporting "Shoreline time series accuracy"). Indeed, the analysis revealed that aerial orthophotos accessed through the National Geoportal exhibit lower planimetric accuracy compared to satellite orthophotos reported on Google Earth. For instance, in Table 3.2, the interquartile range (IQR) of the distance matrices for WMS images was about 2.5 m, while Google Earth images showed significantly higher precision with an IQR of about 0.7 m. Likewise, standard deviation (σ) values highlighted greater variability in WMS imagery (about 1.3 m) compared to Google Earth imagery (0.4 m). Approximately 5700 vertices were validated, with a majority distance of $\approx$ 3.9 m; coherently, the average distance indicates a similar performance with an average value of 8.4 m. The IQR was 7.3 m on average, and the standard deviation of the distances was 5.7 m on average. The dataset used for this validation is freely available in the repository at the following link: https://zenodo.org/records/14711106.

**Table 2**
The percentages of measurements acquired from different satellite platforms are presented for the multidecadal (M), seasonal (S), and total (multidecadal plus seasonal, Tot) time series. The columns correspond to the satellite datasets: Landsat (LS), and Planetscope (PS) for the sandy beaches of Vendicari (VD and San Giorgio (SG).

| | VD | | SG | |
|---|---|---|---|---|
| | LS | PS | LS | PS |
| M | 0.83 | 0.30 | 0.86 | 0.32 |
| S | 0.59 | 1.00 | 0.69 | 0.98 |
| Tot | 0.72 | 0.61 | 0.78 | 0.62 |

**Table 3**
Statistical values characterizing the distance between digitized vertices and shorelines extracted using the IM.

| Month | 05/2022 | 04/2023 |
|---|---|---|
| Time distance (days) | 4 | 0 |
| Vertex numerosity | 287 | 223 |
| IQR (m) | 3.47 | 3.90 |
| *Mo* (m) | 0.14 | 0.45 |
| μ (m) | 3.73 | 5.16 |
| σ (m) | 3.35 | 3.07 |

The San Giorgio Beach exhibits significant fluctuations in the metric values. Each class manifests different frequencies of changes at San Giorgio Beach (Figs. 11 and 3D1). Class J1, J2 and J3 comprise 3800, 456 and 266 measurements, respectively. Additionally, the lengths of each class offer an understanding of the spatial extent of these variations. Class J1 spans 10,000 m, Class J2 covers 1300 m, and Class J3 extends over 700 m. The total length measures 12,000 m, representing the cumulative extent of the observed changes at San Giorgio Beach.

As mentioned earlier, this analysis is based on a comprehensive dataset comprising 38 products, covering a period of 38 years and this extensive dataset allows for a thorough examination of the long-term variations in beach morphology, as captured through the multidecadal analysis at San Giorgio Beach.

The velocities of the displacement fronts are depicted through the processing of the displacement map by quantifying the yearly displacement gradient. The study analyzes coastal dynamics, focusing on sediment accumulation and erosion through high-resolution aerial and satellite orthophotos, alongside multi-decadal shoreline time series. At Marina di Patti, sediment deposition progressively filled southeastern groynes, advancing southeastward between 1989 and 2017. Simultaneously, San Giorgio (Fig. 12) experienced coastal regression characterized by erosion patterns migrating southeastward. Displacement gradients and patterns revealed a dynamic interplay between sediment deposition at Marina di Patti and erosion at San Giorgio. By 2020–2022, sediment accumulation at newly installed groynes in San Giorgio diminished, underscoring the evolving nature of these coastal processes. The displacements identified through high spatial resolution aerial and satellite orthophotos corroborate the displacement patterns and annual displacement gradients derived from the analysis of the multi-decadal time series of the shoreline derived from the Landsat USGS archive. Fig. 13 shows the evolution of the San Giorgio beach sector from 2003 to 2022. For a more detailed description of the process refer to paragraph "Comparative geomorphic overview of San Giorgio and Marina di Patti beaches" in the Supplementary Materials (S.4).

## 4. Discussion

This study demonstrates how the IM through the multi-resolution time series analysis can unravel coastal dynamics across different temporal and spatial scales. Our findings highlight the complementary usefulness of high- and low-resolution data in understanding both

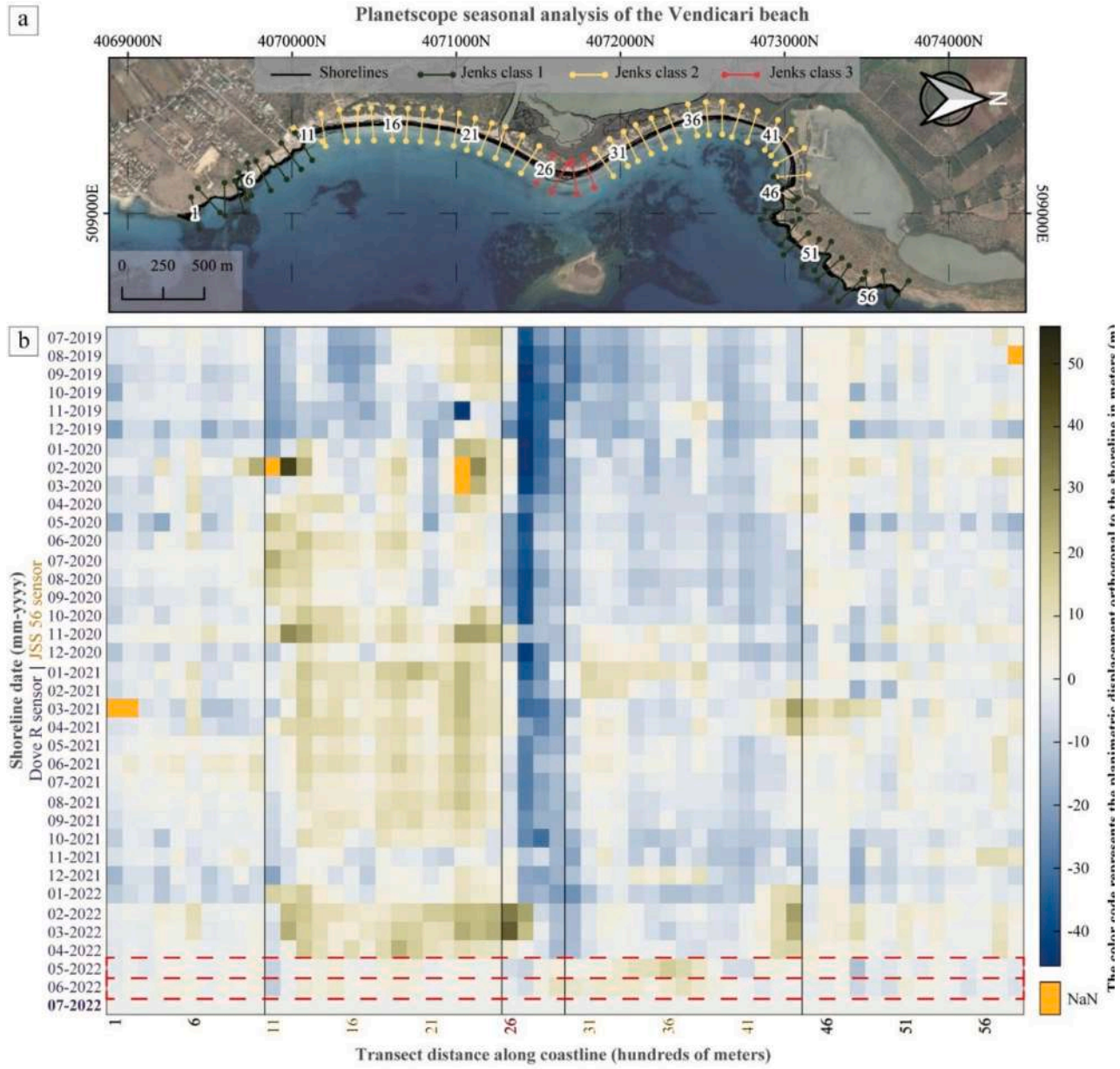


**Fig. 9.** A) The Vendicari beach study site analysed using Planetscope satellite products acquired from July 2019 to July 2022. The colour code of shoreline perpendicular transects is based on the Jenks natural breaks classification variance. B) Heatmap in which each cell represents the along transect shift value measured from each shoreline to the landmark. The orange cells represent points of method criticality. The date is shown on the y-axis, while the x-axis shows the progressive distance along the shoreline. The vertical black represents the limits obtained by applying the Jenks algorithm. The red dashed boxes highlight outliers identified via the pairwise analysis (Fig. 6). (For interpretation of the references to colour in this figure legend, the reader is referred to the web version of this article.)

immediate morphological responses and long-term evolutionary trends. Through systematic analysis of two contrasting sites, we identify key patterns in shoreline behaviour and their implications for both geological interpretation and coastal management.

### 4.1. *Decoding shoreline dynamics through multi-resolution time series*

The application of time series analysis at different resolutions provides insights into both short-term processes and long-term coastal evolutionary patterns. Our validation reveals that while manual digitisation captures instantaneous swash positions, the IM identifies a stable morphological feature between the low tide terrace and the berm, aligning with observations on water diffuse attenuation (Ciraolo et al., 2006) in the near-infrared spectrum as discussed by Caldareri et al. (2024). This distinction helps separate ephemeral water boundaries from actual morphological changes. This discrepancy is particularly evident in high-resolution images, where the planimetric distance between the low tide terrace and the berm exceeds the spatial resolution. The multidecadal (Landsat, Fig. 11) analysis demonstrates effectiveness in capturing long-term trends with consistent subpixel accuracy. The comparison between resolutions reveals that while high-resolution data captures full shoreline variability, lower-resolution observations highlight underlying trends, showing a “dampening effect” that helps distinguish between regular morphological cycles, extreme events, and progressive evolutionary trends (Barnard et al., 2015; Vos et al., 2023).

### 4.2. *Temporal patterns and coastal dynamics*

The correlation analysis reveals distinct temporal signatures at different scales, with a general decrease in correlation over increasing

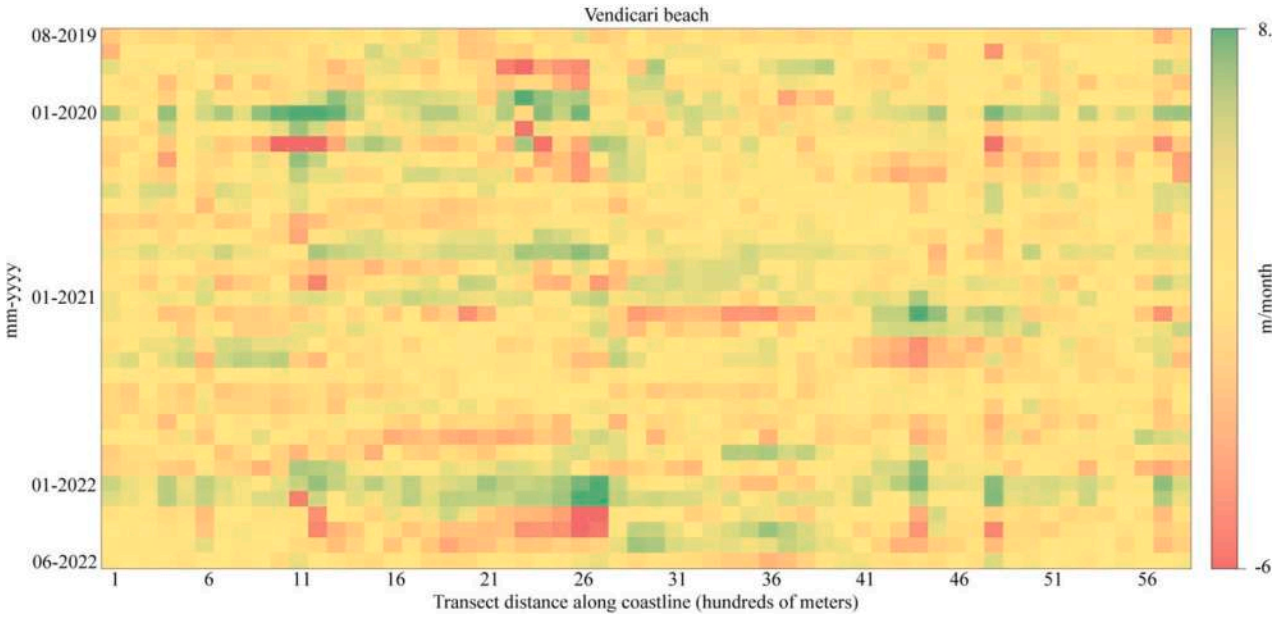


**Fig. 10.** Monthly gradient (m/month) calculated over a 3-month moving windows along the transect on the seasonal time series. The date is shown on the y-axis, while the x-axis shows the progressive distance along the shoreline. The colour scale varies between a minimum percentile set at 3 % (−6.5 m/month) and a maximum percentile set at 97 % (8.0 m/month).

**Table 4**
Orthophotos planimetric accuracy: statistical values characterizing the distance between digitized GCPs.

| | Aerial Orthophoto | Satellite orthophotos | All |
|---|---|---|---|
| $\overline{IQR}(m)$ | 2.54 | 0.68 | 2.35 |
| $\overline{M_0}(m)$ | 1.59 | 0.24 | 0.24 |
| $\overline{\mu}(m)$ | 3.44 | 0.70 | 2.49 |
| $\overline{\sigma}(m)$ | 1.26 | 0.36 | 1.41 |

time lag (Fig. 6). At Vendicari, low correlations in May-June 2022 coincide with the presence of beached *Posidonia Oceanica* deposits or anthropic structures which generate abrupt changes in the shoreline trend. The San Giorgio multidecadal analysis shows a major shift around 2021, suggesting the coastal system reached a critical threshold, possibly due to post-2003 coastal defences (Figs. 11 and 13). Seasonal correlations decrease more rapidly with time lag compared to multi-decadal ones, indicating short-term variations oscillate around more stable long-term trends (Fig. 6). Coastal sectors with similar exposure and sediment characteristics show similar correlation patterns, demonstrating how local morphological conditions could influence environmental response. Variations in the temporal consistency of the data highlight the importance of time series, which allow residual errors to be highlighted and exceptional events to be better identified by explaining the evolution of natural environments in greater detail (Ghaderpour et al., 2023).

### 4.3. Spatial patterns and morphodynamics implications

The Jenks classification analysis reveals distinct spatial patterns related to coastal morphology. At Vendicari, low variance classes (Jenks 1) at beach extremities indicate stability zones, while highest variability (Jenks 3) coincides with the cuspidate salient near Vendicari island (Fig. 9). Transects with intermediate variance (Jenks 2) are located within the two bays. High variance between transects 26–29, combined with maximum gradients, suggests enhanced morphodynamics sensitivity, likely due to relatively shallower depths and increased energy in the sedimentary environment. The two bays flanking the tombolo feature marshes along the shoreline, with wave refraction and diffraction influencing the alongshore N-S current in correspondence of the littoral salient (F. 277 Noto – C.N.R. – M.U.R.S.T., 1997). Notable sedimentation events occurred at transects 23–24 during February-March 2019/2022 and October-November 2019, corresponding to the larger marsh. While the central littoral portion shows sedimentation, the southern bay experiences erosion and shoreline transgression, contrasting with the northern bay's slight regression due to sedimentation. San Giorgio shows different dynamics influenced by anthropic modifications, with coastal defences creating distinct morphodynamic cells (Fig. 11). The shoreline's transformation from linear to sinuous after 2003 demonstrates how artificial structures alter natural evolution patterns, resulting in beach loss up to 120 m in some sectors. Climate change has intensified coastal erosion through more intense storm surges, while anthropization, including road construction and harbour development, has disrupted natural sediment transport patterns highlighting the need to implement these tools to exploit their potential for preventive purposes in coastal environments (Ghaderpour et al., 2023;

**Table 5**
Statistical values characterizing the distance between digitized vertices and shorelines extracted using the IM.

| Year | 1997 | 1999 | 2005 | 2010 | 2012 | 2014 | 2017 | 2018 | 2020 |
|---|---|---|---|---|---|---|---|---|---|
| Time distance (days) | <20 | 3 | 12 | 4 | 2 | 49 | 49 | 40 | 62 |
| Vertex numerosity | 357 | 511 | 944 | 771 | 791 | 333 | 749 | 408 | 1214 |
| IQR (m) | 9.59 | 9.23 | 9.67 | 6.71 | 5.72 | 7.68 | 6.95 | 6.42 | 5.28 |
| *Mo* (m) | 14.83 | 7.13 | 5.97 | 0.51 | 3.90 | 5.90 | 2.40 | 4.78 | 0.55 |
| μ (m) | 13.34 | 12.86 | 13.34 | 6.17 | 6.42 | 8.05 | 7.74 | 6.83 | 5.89 |
| σ (m) | 6.81 | 6.41 | 6.67 | 4.50 | 4.32 | 6.62 | 6.45 | 5.40 | 5.29 |

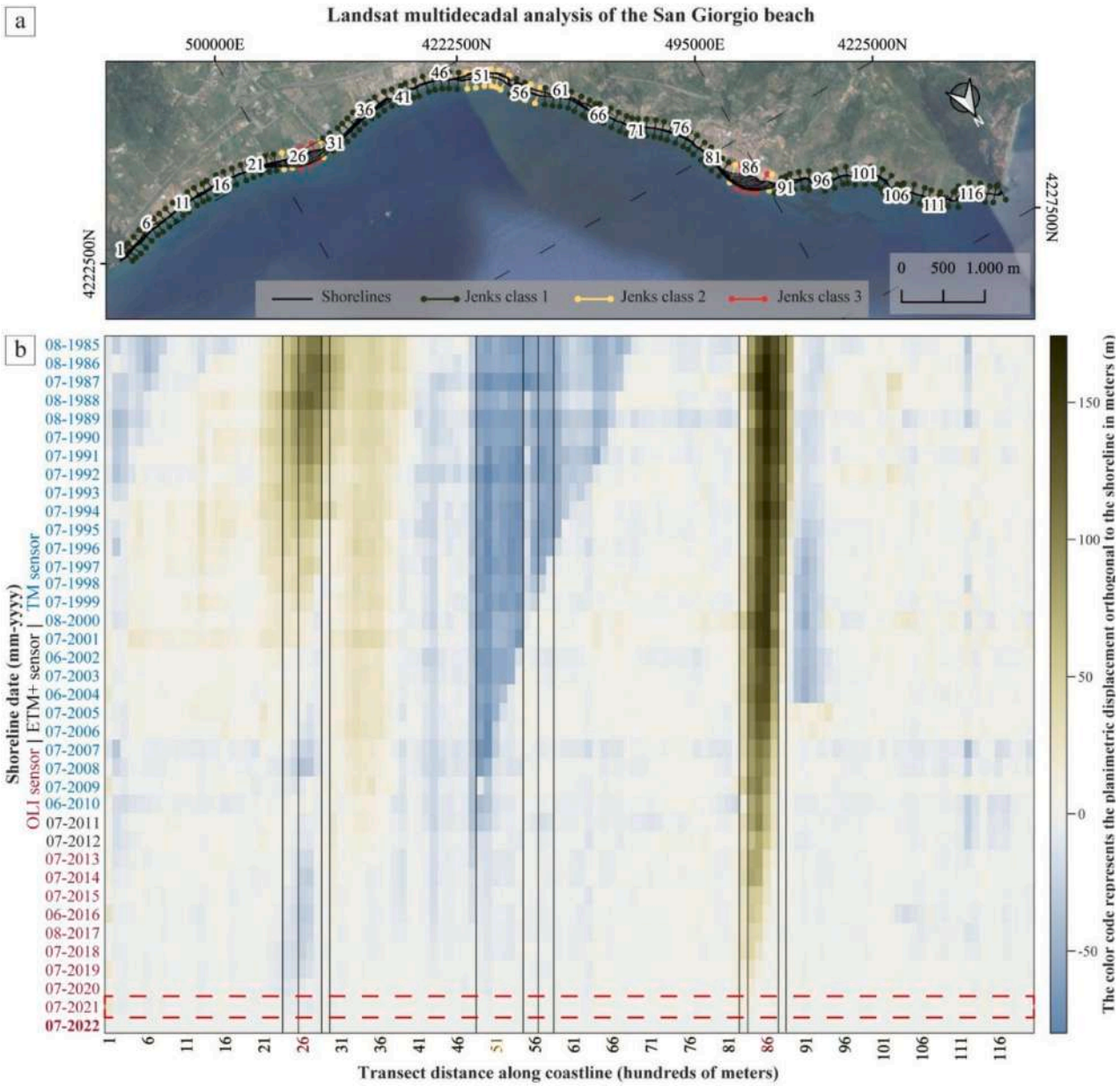


**Fig. 11.** A) The San Giorgio Beach study site which we analysed extracting shorelines using Landsat satellite products, from 1985 to 2022. The colour code of shoreline perpendicular transects is based on the Jenks natural breaks classification variance. B) Heatmap in which each cell represents the horizontal shift value measured from each shoreline to the landmark. The date is shown on the y-axis, while the x-axis shows the progressive distance along the shoreline. The vertical black represents the limits obtained by applying the Jenks algorithm. The red dashed boxes highlight outliers identified via the pairwise analysis (Fig. 6). (For interpretation of the references to colour in this figure legend, the reader is referred to the web version of this article.)

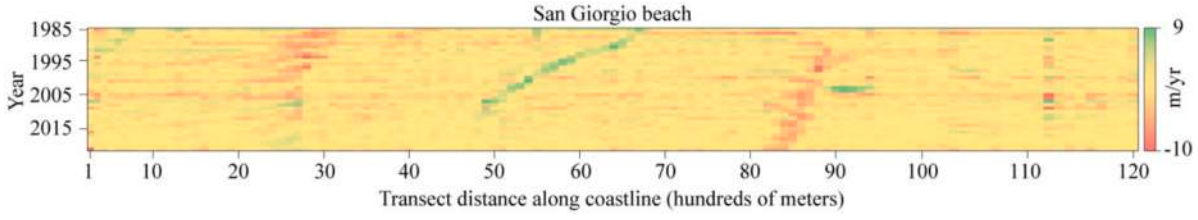


**Fig. 12.** Yearly gradient (m/year) calculated over a 3-year moving window along the transect on the multidecadal time series. The date is shown on the y-axis, while the x-axis shows the progressive distance along the shoreline. The colour scale varies between a minimum percentile set at 2 % (−10 m/year) and a maximum percentile set at 98 % (9 m/year).

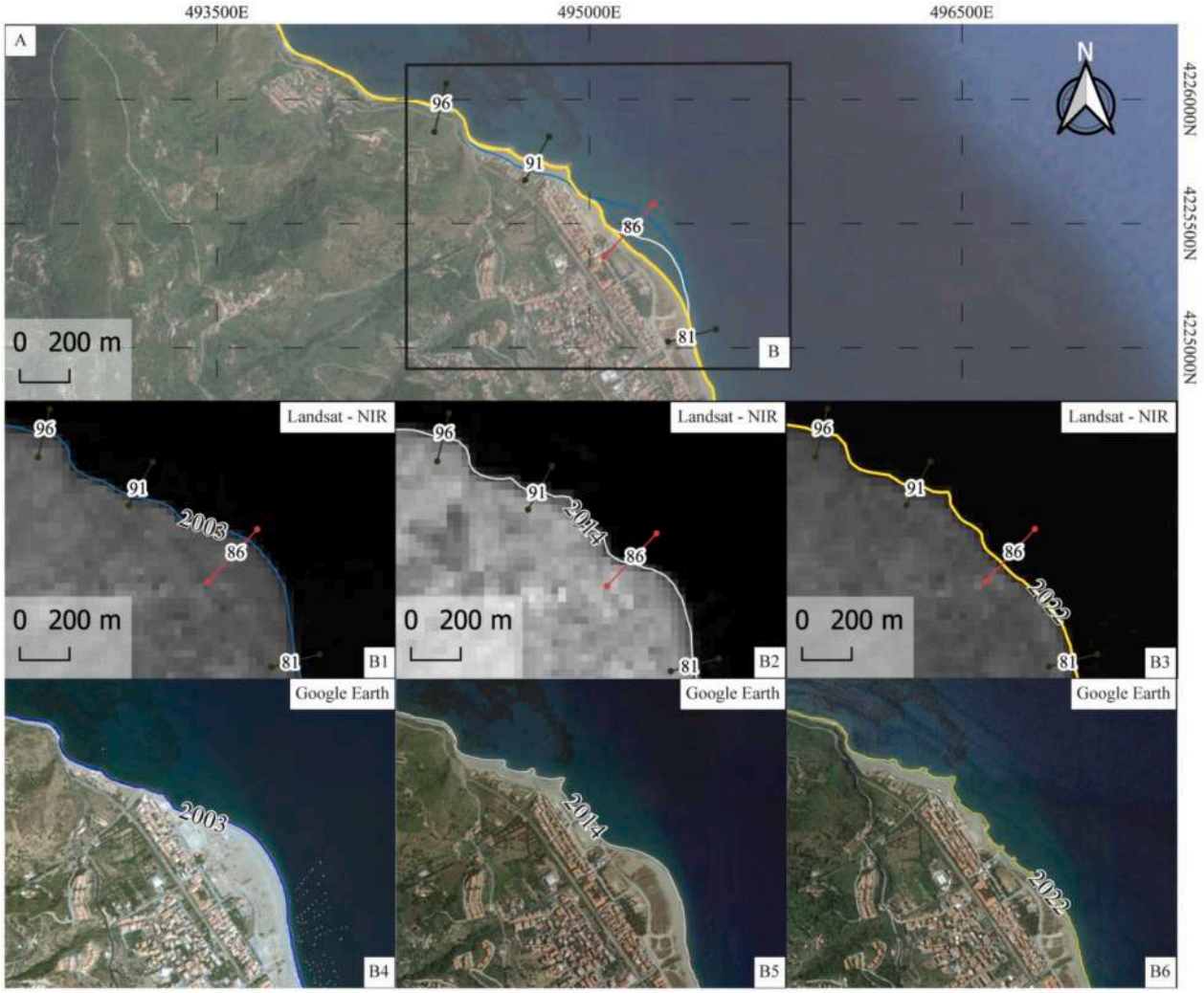


**Fig. 13.** A) Evolution of the shoreline in the San Giorgio sector with Google Earth base map. The 2003 extracted shoreline is shown in blue; in white the one of 2014 and in yellow the shoreline of 2022. Numbered coast perpendicular lines represent the transect as per Fig. 11. B1-B3) Zoom area shown in the subsequent insets with a Landsat base map, in which the shoreline changes resulting from the groynes coastal defence built since 2003. B4-B6) Insets shown the same sector with a Google Earth base map. (For interpretation of the references to colour in this figure legend, the reader is referred to the web version of this article.)

Randazzo and Lanza, 2020).

### 4.4. Decoding drivers of coastal landscape evolution

The study sites demonstrate the interplay between natural processes and anthropic modifications. Vendicari, minimally influenced by human activity, shows natural drivers dominating evolution patterns, with regular events modulated by local geological setting. Significant shoreline transgressions occur in December, coinciding with winter solstice high tides. Paroxysmal climatic events can cause simultaneous erosion and sedimentation in different areas (Short, 1999), influenced by coastal geometry and the angle between the coast and main currents (Bascom, 1951; Short, 1999). San Giorgio reveals how anthropic interventions can fundamentally alter natural patterns, with coastal defences triggering cascading morphological adjustments. The analysis reveals a hierarchy of drivers: seasonal astronomical and meteorological forcing create regular patterns modulated by local conditions, while decadal-scale sediment transport processes drive shoreline dynamics, susceptible to anthropic modifications.

### 4.5. Implications for Quaternary geology and coastal management

Our time series analysis offers a dual contribution to coastal studies. From a geological perspective, the quantification of modern shoreline behaviour provides crucial insights for interpreting Quaternary deposits through the principle of actualism. The natural variability ranges observed at Vendicari (−45 m to + 56 m) establish quantitative baselines for interpreting past coastal changes, while the distinctive signatures of anthropic modifications at San Giorgio offer modern analogues for understanding Anthropocene geological records. This framework helps to interpret cyclic sedimentary deposits and abrupt transitions in the geological record, particularly valuable for distinguishing between periodic (tidal), episodic (storm), and progressive (evolutionary) changes preserved in coastal sequences. From a monitoring and management perspective, our systematic analysis of temporal signatures and process thresholds provides a robust framework for coastal assessment. The demonstrated effectiveness of multi-resolution analysis in capturing both immediate responses and long-term trends can rationalise coastal monitoring strategies. San Giorgio's case particularly highlights how this approach can assess anthropic impacts and forecast potential morphological adjustments, essential for informed coastal management decisions. The characterization of satellite product sensitivity opens new possibilities for analysing coastal sedimentary dynamics in relation to tidal regimes (Caldareri et al., 2024; Maltese et al., 2024). The heatmaps produced in this study can provide valuable information about tidal cyclicity and intensity. Rapid analyses at the physiographic unit scale

could reveal relationships with tidal currents, potentially contributing to the assessment of tidal energy potential in coastal areas. However, this would require expanding the current dataset with satellite products providing more frequent revisit times for detailed tidal analysis.

### 4.6. Limitations and future developments

This study strategically focuses on evaluating coastal dynamics in areas with homogeneous tidal regimes and similar coastal settings, building on the research by Caldareri et al. (2024), in which the IM was developed and validated on sandy beaches along the Sicilian coast characterized by microtidal regimes. We selected multiple study sites with similar tidal characteristics to systematically test and demonstrate the IM's reliability and reproducibility within this well-defined environmental context. This methodological design enhances the possibility of establishing baseline performance metrics for the technique. The results obtained in these controlled settings provide a strong foundation for future research, which will expand the IM's application to diverse tidal regimes and heterogeneous coastline environments, further demonstrating its versatility and robustness across a broader spectrum of coastal settings.

## 5. Conclusions

This study evaluated the effectiveness of the IM for characterizing shoreline dynamics through time series analysis. The method was applied to about 150 multispectral satellite images spanning about 40 years across two study sites along the coast of the Sicilian Island in the central Mediterranean Sea, demonstrating its reliability with different resolution datasets. Our accuracy assessment, based on manually digitised shorelines from high-resolution archival images, revealed that while seasonal analysis shows vertex positions at subpixel distances from IM-extracted lines, their average distance exceeds spatial resolution. This difference arises from visual digitization capturing the swash uprush, while the isoradiometric shoreline identifies a more stable feature between the low tide terrace and the berm. This discrepancy is evident in high-resolution images (Planetscope) but becomes negligible in lower-resolution time series (Landsat), where all indices indicate subpixel accuracy. The analysis of different resolution datasets revealed distinct variability ranges, highlighting the importance of considering spatial resolution when comparing shoreline shifts. The pair analysis conducted on 11,900 pairs of shift measurements allowed us to identify 219 outliers (interpreted as method criticalities), 137 measurements linked to paroxysmal events, and 11,544 measurements associated with the normal variability of the shoreline at each analyzed site. High-resolution products capture finer coastal details and nuances, while lower-resolution data smooth out subtle variations. This finding emphasizes the necessity of pair analysis when developing new shoreline evolution time series methods. Furthermore, we calculated the gradient of the shifts to quantify the rate of change in shoreline position. Our analysis revealed a peak average positive gradient of 13.15 m/yr, indicating the highest rate of seaward movement or accretion observed. The average positive gradient was 1.22 m/yr. We also identified a maximum negative gradient of −5.38 m/yr, representing the greatest rate of landward movement or erosion recorded, with the average negative gradient being −0.63 m/yr.The methodology demonstrated a dual utility: as a tool for interpreting Quaternary geological processes through the principle of actualism, and as a framework for rationalizing shoreline monitoring and coastal management strategies. The obtained results have proved valuable both in establishing modern analogues for geological interpretation and in assessing anthropic impacts on coastal areas. Future research will focus on advancing statistical and methodological analyses, particularly in the selection and characterization of paroxysmal events from the broader set of outliers, enhancing our ability to interpret both geological records and contemporary coastal dynamics.

## CRediT authorship contribution statement

**F. Caldareri:** Writing – review & editing, Writing – original draft, Visualization, Validation, Methodology, Investigation, Data curation, Conceptualization. **N. Parrino:** Writing – review & editing, Writing – original draft, Visualization, Validation, Methodology, Investigation, Formal analysis, Data curation, Conceptualization. **L. Balsamo:** Writing – review & editing, Visualization, Validation, Data curation. **G. Dardanelli:** Writing – review & editing, Validation, Data curation. **S. Todaro:** Writing – review & editing, Visualization, Validation. **A. Sulli:** Writing – review & editing, Supervision, Project administration, Funding acquisition. **A. Maltese:** Writing – review & editing, Writing – original draft, Visualization, Validation, Supervision, Methodology, Investigation, Formal analysis, Data curation, Conceptualization.

## Funding

This research is funded by European Union – NextGenerationEU – Mission 4 "Education and Research" – Component 2 "From Research to Business" – Investment 3.1 "Fund for the realization of an integrated system of research and innovation infrastructures" – Project IR0000037 – GeoSciences IR.

## Declaration of competing interest

The authors declare that they have no known competing financial interests or personal relationships that could have appeared to influence the work reported in this paper.

## Acknowledgements

Planetscope images were made available by Planet Labs Inc. (San Francisco, CA) within the Planet's Education and Research (E&R) Program.

## Appendix A. Supplementary data

Supplementary data to this article can be found online at https://doi.org/10.1016/j.jag.2025.104618.

## Data availability

Data will be made available on request.

## References

Aedla, R., Dwarakish, G.S., Reddy, D.V., 2015. Automatic Shoreline Detection and Change Detection Analysis of Netravati-GurpurRivermouth Using Histogram Equalization and Adaptive Thresholding Techniques. Aquat. Procedia 4, 563–570. https://doi.org/10.1016/j.aqpro.2015.02.073.

Agate, M., Antonioli, F., Caldareri, F., Devoto, S., Morticelli, M.G., Sulli, A., Parrino, N., Furlani, S., 2024. Decoding Late Quaternary faulting through marine terraces and MIS 5.5 tilted tidal notches: Insights from central Mediterranean Sea (NW Sicily, Italy). Geomorphology 472, 109587. https://doi.org/10.1016/j.geomorph.2024.109587.

Almeida, L.P., Efraim De Oliveira, I., Lyra, R., Scaranto Dazzi, R.L., Martins, V.G., Da Fontoura, H., Klein, A., 2021. Coastal Analyst System from Space Imagery Engine (CASSIE): Shoreline management module. Environ. Model. Softw. 140, 105033. https://doi.org/10.1016/j.envsoft.2021.105033.

Barnard, P.L., Short, A.D., Harley, M.D., Splinter, K.D., Vitousek, S., Turner, I.L., Allan, J., Banno, M., Bryan, K.R., Doria, A., Hansen, J.E., Kato, S., Kuriyama, Y., Randall-Goodwin, E., Ruggiero, P., Walker, I.J., Heathfield, D.K., 2015. Coastal vulnerability across the Pacific dominated by El Niño/Southern Oscillation. Nature Geosci 8, 801–807. https://doi.org/10.1038/ngeo2539.

Bascom, W.M., 1951. The relationship between sand size and beach-face slope. Eos. Trans. AGU 32 (6), 866–874. https://doi.org/10.1029/TR032i006p00866.

Benetazzo, A., Barbariol, F., Davison, S., 2020. Short-Term/Range Extreme-Value Probability Distributions of Upper Bounded Space-Time Maximum Ocean Waves. JMSE 8, 679. https://doi.org/10.3390/jmse8090679.

Bengoufa, S., Niculescu, S., Mihoubi, M.K., Belkessa, R., Abbad, K., 2021. Rocky shoreline extraction using a deep learning model and object-based image analysis.

Int. Arch. Photogramm. Remote Sens. Spatial Inf. Sci. XLIII-B3-2021, 23–29. doi: 10.5194/isprs-archives-XLIII-B3-2021-23-2021.
Boussetta, A., Niculescu, S., Bengoufa, S., Mejri, H., Zagrarni, M.F., 2023. Assessment of Coastal Vulnerability to Erosion Risk Using Geospatial and Remote Sensing Methods (Case of Jerba Island, Tunisia). In: Niculescu, S. (Ed.), European Spatial Data for Coastal and Marine Remote Sensing. Springer International Publishing, Cham, pp. 113–132. https://doi.org/10.1007/978-3-031-16213-8_7.
Burbank, D.W., Anderson, R.S., 2013. Tectonic Geomorphology, Second Edition. Environmental & Engineering Geoscience 19, 198–200. doi: 10.2113/gseegeosci.19.2.198.
Burningham, H., Fernandez-Nunez, M., 2020. Shoreline change analysis, in: Sandy Beach Morphodynamics. Elsevier, pp. 439–460. doi: 10.1016/B978-0-08-102927-5.00019-9.
Caldareri, F., Sulli, A., Parrino, N., Dardanelli, G., Todaro, S., Maltese, A., 2024. On the shoreline monitoring via earth observation: An isoradiometric method. Remote Sens. Environ. 311, 114286. https://doi.org/10.1016/j.rse.2024.114286.
Chen, C., Liang, J., Xie, F., Hu, Z., Sun, W., Yang, G., Yu, J., Chen, L., Wang, L., Wang, L., Chen, H., He, X., Zhang, Z., 2022. Temporal and spatial variation of shoreline using remote sensing images for Zhoushan archipelago, China. Int. J. Appl. Earth Obs. Geoinf. 107, 102711. https://doi.org/10.1016/j.jag.2022.102711.
C.N.R. - M.U.R.S.T., 1997 - Atlante delle spiagge italiane - Dinamismo, tendenza evolutiva, opere umane. 108 Fogli in Scala 1:100.000, SELCA, Firenze. ISBN: 97888CNR09.
Ciraolo, G., Cox, E., La Loggia, G., Maltese, A., 2006. The classification of submerged vegetation using hyperspectral MIVIS data. Ann. Geophys. 49 (1). https://doi.org/10.4401/ag-3152.
Costantino, D., Pepe, M., Dardanelli, G., Baiocchi, V., 2020. Using optical satellite and aerial imagery for automatic coastline mapping. Geographia Technica 15. https://doi.org/10.21163/GT_2020.152.17.
D'Agostino, R.B., Stephens, M.A., 1986. *Goodness-of-Fit Techniques*. Marcel Dekker, New York.
Gao, B., 1996. NDWI—A normalized difference water index for remote sensing of vegetation liquid water from space. Remote Sens. Environ. 58, 257–266. https://doi.org/10.1016/S0034-4257(96)00067-3.
Gens, R., 2010. Remote sensing of shorelines: detection, extraction and monitoring. Int. J. Remote Sens. 31 (7), 1819–1836. https://doi.org/10.1080/01431160902926673.
Ghaderpour, E., Mazzanti, P., Mugnozza, G.S., Bozzano, F., 2023. Coherency and phase delay analyses between land cover and climate across Italy via the least-squares wavelet software. International Journal of Applied Earth Observation and Geoinformation 118, 103241. https://doi.org/10.1016/j.jag.2023.103241.
Hannv, Z., Qigang, J., Jiang, X., 2013. Coastline Extraction Using Support Vector Machine from Remote Sensing Image. J. Multimed. 8. https://doi.org/10.4304/jmm.8.2.175-182.
https://gn.mase.gov.it/portale/servizio-di-consultazione-wms.
https://www.usgs.gov/media/files/landsat-collection-1-vs-collection-2-summary.
Jenks, G.F., Caspall, F.C., 1971. Error on choroplethic maps: definition, measurement, reduction. Annals of the Association of American Geographers 61 (2), 217–244. https://doi.org/10.1111/j.1467-8306.1971.tb00779.x.
Kotz, S., Nadarajah, S., 2015. Extreme value distributions: theory and applications, Reprinted. ed. Imperial College Press, London.
Luijendijk, A., Hagenaars, G., Ranasinghe, R., Baart, F., Donchyts, G., Aarninkhof, S., 2018. The State of the World's Beaches. Sci. Rep. 8, 6641. https://doi.org/10.1038/s41598-018-24630-6.
Maltese, A., Caldareri, F., Dardanelli, G., Todaro, S., Parrino, N., Sulli, A., 2024. On the shoreline positioning via remote sensing imagery: an isoradiometric approach. J. Appl. Remote Sens. 18 (1), 014529. https://doi.org/10.1117/1.JRS.18.014529.
Maltese, A., Caldareri, F., Parrino, N., Todaro, S., Dardanelli, G., Sulli, A., 2023. A radiometric contouring approach to map the shoreline, in: Remote Sensing for Agriculture, Ecosystems, and Hydrology XXV. Presented at the Remote Sensing for Agriculture, Ecosystems, and Hydrology XXV, SPIE, pp. 57–66. doi: 10.1117/12.2690731.
Masselink, G.; Short, A. D., 1993. The effect of tidal range on beach morphodynamics and morphology: a conceptual beach model. Journal of Coastal Research. 9 (3): 785–800. ISSN 0749-0208. http://www.jstor.org/stable/4298129.
McFeeters, S.K., 2013. Using the Normalized Difference Water Index (NDWI) within a Geographic Information System to Detect Swimming Pools for Mosquito Abatement: A Practical Approach. Remote Sens. (Basel) 5, 3544–3561. https://doi.org/10.3390/rs5073544.
Murray, J., Adam, E., Woodborne, S., Miller, D., Xulu, S., Evans, M., 2023. Monitoring Shoreline Changes along the Southwestern Coast of South Africa from 1937 to 2020 Using Varied Remote Sensing Data and Approaches. Remote Sens. (Basel) 15 (2), 317. https://doi.org/10.3390/rs15020317.
Otsu, N., 1979. A Threshold Selection Method from Gray-Level Histograms. IEEE Trans. Syst. Man, Cybern. 9, 62–66. https://doi.org/10.1109/TSMC.1979.4310076.
Ouyang, Y., Chong, J., Wu, Y., 2010. Two coastline detection methods in Synthetic Aperture Radar imagery based on Level Set Algorithm. Int. J. Remote Sens. 31, 4957–4968. https://doi.org/10.1080/01431161.2010.485142.
Palomar-Vázquez, J., Pardo-Pascual, J.E., Almonacid-Caballer, J., Cabezas-Rabadán, C., 2023. Shoreline Analysis and Extraction Tool (SAET): A New Tool for the Automatic Extraction of Satellite-Derived Shorelines with Subpixel Accuracy. *Remote Sens. (Basel)* 15 (12), 3198. https://doi.org/10.3390/rs15123198.
Pardo-Pascual, J.E., Sánchez-García, E., Almonacid-Caballer, J., Palomar-Vázquez, J.M., Priego de los Santos, E., Fernández-Sarría, A., Balaguer-Beser, Á., 2018. Assessing the Accuracy of Automatically Extracted Shorelines on Microtidal Beaches from Landsat 7, Landsat 8 and Sentinel-2 Imagery. Remote Sens. (Basel) 10 (2), 326. https://doi.org/10.3390/rs10020326.
Parrino, N., Burrato, P., Sulli, A., Gasparo Morticelli, M., Agate, M., Srivastava, E., Malik, J.N., Di Maggio, C., 2023. Plio-Quaternary coastal landscape evolution of north-western Sicily (Italy). J. Maps 19 (1), 1–13. https://doi.org/10.1080/17445647.2022.2159889.
Parrino, N., Pepe, F., Burrato, P., Dardanelli, G., Corradino, M., Pipitone, C., Morticelli, M.G., Sulli, A., Di Maggio, C., 2022. Elusive active faults in a low strain rate region (Sicily, Italy): Hints from a multidisciplinary land-to-sea approach. Tectonophysics 839, 229520. https://doi.org/10.1016/j.tecto.2022.229520.
Pipitone, C., Maltese, A., Dardanelli, G., Lo Brutto, M., La Loggia, G., 2018. Monitoring Water Surface and Level of a Reservoir Using Different Remote Sensing Approaches and Comparison with Dam Displacements Evaluated via GNSS. Remote Sens. (Basel) 10 (1), 71. https://doi.org/10.3390/rs10010071.
Planet Labs PBC, Planet, Planet Application Program Interface: In Space for Life on Earth, 2019—2022, https://api.planet.com.
Randazzo, G., Lanza, L., 2020. Regional Plan against Coastal Erosion: A conceptual model for Sicily. Land 9, 307. https://doi.org/10.3390/land9090307.
Sharma, R.C., Tateishi, R., Hara, K., Nguyen, L.V., 2015. Developing Superfine Water Index (SWI) for Global Water Cover Mapping Using MODIS Data. Remote Sens. (Basel) 7, 13807–13841. https://doi.org/10.3390/rs71013807.
Short, A.D., 1999. Handbook of beach and shoreface morphodynamics. John Wiley, Great Britain.
Srivastava, E., Malik, J.N., Parrino, N., Burrato, P., Sharma, N., Gadhavi, M., Sulli, A., Di Maggio, C., Morticelli, M.G., 2023. Extremely fast Holocene coastal landscape evolution in the Kachchh Upland (NW India): Clues from a multidisciplinary review. J. Maps 19 (1), 1–10. https://doi.org/10.1080/17445647.2023.2167617.
Toure, S., Diop, O., Kpalma, K., Maiga, A.S., 2019. Shoreline Detection using Optical Remote Sensing: A Review. ISPRS Int. J. Geo Inf. 8, 75. https://doi.org/10.3390/ijgi8020075.
Toure, S., Diop, O., Kpalma, K., Maiga, A.S., 2018. Coastline detection using fusion of over segmentation and distance regularization level set evolution. Int. Arch. Photogramm. Remote Sens. Spatial Inf. Sci. XLII-3/W4, 513–518. https://doi.org/10.5194/isprs-archives-XLII-3-W4-513-2018.
USGS, 2017. Landsat Collection 2 Level 2 Tier 1 Product Definition, https://www.usgs.gov/landsat-missions/landsat-collection-2-level-2-science-products.
Vos, K., Splinter, K.D., Harley, M.D., Simmons, J.A., Turner, I.L., 2019a. CoastSat: A Google Earth Engine-enabled Python toolkit to extract shorelines from publicly available satellite imagery. Environ. Model. Softw. 122, 104528. https://doi.org/10.1016/j.envsoft.2019.104528.
Vos, K., Harley, M.D., Splinter, K.D., Simmons, J.A., Turner, I.L., 2019b. Sub-annual to multi-decadal shoreline variability from publicly available satellite imagery. Coast. Eng. 150, 160–174. https://doi.org/10.1016/j.coastaleng.2019.04.004.
Vos, K., Splinter, K.D., Palomar-Vázquez, J., Pardo-Pascual, J.E., Almonacid-Caballer, J., Cabezas-Rabadán, C., Kras, E.C., Luijendijk, A.P., Calkoen, F., Almeida, L.P., Pais, D., Klein, A.H.F., Mao, Y., Harris, D., Castelle, B., Buscombe, D., Vitousek, S., 2023. Benchmarking satellite-derived shoreline mapping algorithms. Commun Earth Environ 4, 1–17. https://doi.org/10.1038/s43247-023-01001-2.
Wicaksono, A., Wicaksono, P., 2019. Geometric Accuracy Assessment for Shoreline Derived from NDWI, MNDWI, and AWEI Transformation on Various Coastal Physical Typology in Jepara Regency using Landsat 8 OLI Imagery in 2018. Geoplanning: Journal of Geomatics and Planning 6, 1, 55–72. https://doi.org/10.14710/geoplanning.6.1.55-72.
Yasir, M., Sheng, H., Fan, H., Nazir, S., Niang, A.J., Salauddin, Md., Khan, S., 2020. Automatic Shoreline Extraction and Changes Analysis Using Remote Sensing and GIS Technology. IEEE Access 8, 180156–180170. https://doi.org/10.1109/ACCESS.2020.3027881.